ARTICLES

Structural Study of Inorganic Oxides in a Hybrid Organic−Inorganic Solid Polymer Electrolyte

Lyudmila M. Bronstein,*,† Earl Ashcraft,† Peter DeSanto, Jr.,‡ Robert L. Karlinsey,† and Josef W. Zwanziger*,†,§

Department of Chemistry, Indiana University, Bloomington, Indiana 47405, and Department of Chemical Engineering, University of Delaware, Newark, Delaware 19716

Received: August 21, 2003; In Final Form: March 11, 2004

Polymer−inorganic composite electrolytes very often show superior properties as compared to simple polymer electrolytes, and this enhancement is often ascribed to the structure and interfacial properties of the composite. Here, the structure of aluminosilica (AlSi) domains formed within organic−inorganic solid polymer electrolytes was studied using solid state ^{29}Si and ^{27}Al magic angle spinning (MAS) NMR, transmission electron microscopy (TEM), and nitrogen sorption experiments following material calcinations, to determine how the composite affects the properties in this class of polymer electrolytes. The major feature of all the calcined AlSi's based on 600 MW poly(ethylene glycol) (PEG) is the presence of two types of morphologies: nanoparticles with sizes of about 20−60 nm, and larger platelike particles. Increasing the amount of AlSi in the organic−inorganic composite material (OICM) increases the fraction of platelike particles relative to nanoparticles. The nanoparticles are practically nonporous, while the platelets are considerably mesoporous. When 100 000 MW poly(ethyelene oxide) is employed instead of low-molecular-weight PEG, the AlSi mainly consists of platelets with no porosity. The BET (Brunauer-Emmet-Teller) surface areas for all the samples are essentially equal to their external surface areas, indicating that pores located inside the AlSi are closed and do not participate in the Li conduction process. An increased fraction of AlSi nanoparticles vs platelets was found to provide higher interfacial surface area and also higher conductivity.

Introduction

Multifunctional hybrid materials combining intimately mixed organic and inorganic components can yield high-performance materials with properties not found in either component individually (see for example the Special Issue of the journal *Chemistry of Materials* devoted to organic−inorganic nanocomposite materials[1−8]). Different kinds of organic homo- and copolymers are commonly used as an organic constituent. In so doing, polymers can be either preformed[7,9,10] or synthesized in situ.[5,11] The choice of the polymer is determined by the properties required. Use of amphiphilic block copolymers allows formation of well-ordered hybrid materials where the inorganic component is normally located in a hydrophilic or polar block.[12,13] Inorganic components can be widely varied and include metal,[14,15] metal oxide,[16−19] and semiconductor nanoparticles[20−22] or various kinds of inorganic networks developed within a polymer component.[23−26] For the latter materials, slight variation in composition or reaction conditions can result in alteration of the material structure. In turn, this alteration opens an excellent opportunity to tailor the properties of these hybrid materials.

Recently organic−inorganic composite materials (OICM) were suggested as solid polymer electrolytes (SPE) for secondary Li batteries.[8,27−35] The OICM may contain an ion-conducting polymer (for example, poly(ethylene oxide) [PEO] or poly(ethylene glycol) [PEG]) coupled with a Li salt and metal oxide fillers of various size and morphology, including mesoporous silica.[28,30,36] PEO can also be covalently attached to the surface of inorganic materials, as described in refs 29,32,37 for organically modified silicas formed by sol−gel reaction of corresponding silanes. Attachment of PEG hydroxyl end groups to the inorganic composite may occur during formation of hybrid SPE due to interaction of silanol[32] and/or glycidyl[8,38] groups with PEG hydroxyl groups. As suggested in a number of publications,[19,34,39−41] a crucial role in the enhanced properties of the hybrid OICM is ascribed to the interface between the organic and inorganic components. For hybrid SPE films, where conductivity strongly depends on the transport of Li ions within the hybrid material, this interface is believed to be especially important.

In our preceding papers we described the structure and properties of an organic−inorganic SPE comprised of two major components: PEO containing Li triflate (LiTf), and organically modified aluminosilica (AlSi) formed by sol−gel reaction of (3-glycidoxypropyl)trimethoxysilane (GLYMO) and Al(tri-*sec*-butoxide).[8,31,42] Condensation of the AlSi within the "PEO + LiTf" phase ensures a fresh AlSi-polymer interface and enhanced conductivity.[8,43] The glycidyl group of GLYMO is

* Authors to whom correspondence should be addressed. E-mail: lybronst@indiana.edu; jzwanzig@dal.ca.
† Indiana University.
‡ University of Delaware.
§ Current address : Department of Chemistry and Institute for Research in Materials, Dalhousie University, Halifax, NS, B3H 4J3 Canada.

10.1021/jp036498j CCC: $27.50
Published on Web 04/17/2004

polymerized in the presence of Al(tri-*sec*-butoxide), which results in (i) compatibility with PEO, and (ii) additional cross-linking within AlSi. Since the properties of AlSi-based SPE strongly depend on the AlSi loading in addition to other parameters,[8] characterization of the OICM structure, i.e., structural study allowing one to assess and to tailor the structure of these SPE, is essential for development of novel efficient Li batteries.

However, characterization of the structure of these materials is a considerable challenge. When the inorganic component of OICM consists of preformed nanoparticles (fillers), their characterization can be easily performed using a variety of techniques designed to assess the particle size and structure.[44] However, when an interface forms in situ within the OICM, it is a very difficult task to obtain reliable data on size and structure of organic and inorganic domains. In a preceding publication,[43] we performed an ^{1}H spin diffusion experiment in an attempt to estimate the size of the mobile PEO domains formed in these OICM. The sizes of the mobile domains calculated from this experiment were about 21, 14, and 4 nm for 40 wt %, 55 wt %, and 70 wt % AlSi in OICM, respectively. At the same time, for the inorganic domain (AlSi), only local structure using solid-state ^{29}Si and ^{27}Al MAS NMR was studied,[8,38,43,45] while the overall structure, including the size of AlSi domains, was unknown. As has been well established, the ordered structure of mesoporous oxides prepared by templating over block copolymer templates well reproduces the structure of the original block copolymer template.[46] The preservation of the precursor material (OICM) structure after calcination was also reported in refs 47,48 for hybrid materials containing analogous AlSi (as in this work) and polyisoprene-*block*-poly(ethylene oxide) as a polymeric component. The goal of this work is an extensive structural study of the AlSi component obtained after calcination of OICM as a key way to assess the structure of aluminosilica domains formed in OICM. This paper reports the data from solid-state NMR, transmission electron microscopy (TEM), and nitrogen adsorption studies of the inorganic component obtained after calcination of OICM based on "PEO + LiTf" and AlSi derived from GLYMO and Al(tri-*sec*-butoxide). The dependence of the AlSi domain structure on the AlSi amount, PEO molecular weight, and method of the SPE film preparation were established.

Experimental Section

Poly(ethylene glycol) (PEG) and poly(ethylene oxide) (PEO) with molecular weights of 600 and 100 000, respectively, were purchased from Aldrich and used as received. Li triflate, THF, aluminum tri-*sec*-butoxide (Aldrich), chloroform (EM Ind., Inc.), and (3-glycidoxypropyl)trimethoxysilane (GLYMO, Fluka) were used without further purification. Water was purified with a "Barnstead NANOpure water" purification system.

Synthesis of OICM based on PEO (PEG) and AlSi was carried out as described elsewhere.[8] In a typical experiment, 0.4 g (9 mmol) of PEO (PEG) in 5 mL of chloroform were mixed with 0.1 g (0.64 mmol) of Li triflate in 5 mL of THF. After 30 min stirring, the solution was set aside. The inorganic part of the hybrid was prepared by hydrolysis of the mixture of GLYMO with Al tri-*sec*-butoxide in the molar ratio 80:20, respectively. Hydrolysis was initiated by addition of 15% of an equimolar amount of water containing HCl (0.01 N solution). After 15-min stirring at ~0 °C (water-ice bath) and 15 min at room temperature, the reaction mixture was charged with the residue of the 0.01 N HCl solution and stirred for 20 min. The prehydrolyzed sol was added to the solution containing PEO (PEG) and Li salt (amount was determined by the desired ratio of PEO/inorganic hybrid, which varied in the range of 40−70 wt %) and stirred for 1 h. Afterward the solvents were evaporated on a Teflon dish at 65−70 °C for 2 h. In other experiments, films were obtained by spin coating at 78 rpm followed by thermal treatment at 60 °C for 2 h. The solid film was further treated at 130 °C in a vacuum for 1 h to complete condensation. Calcination was carried out at 500 °C for 4 h in nitrogen and for 12 h in oxygen.

In this paper the following notations are used: PEG6-40 stands for OICM based on 600 MW PEG and 40 wt % AlSi. PEG6-55 and PEG6-70 are OICM based on 600 MW PEG and 55 and 70 wt % AlSi, respectively. PEO1000-55 stands for OICM based on 100 000 MW PEO and 55 wt % AlSi. AlSi-(6-40) stands for calcined aluminosilica based on 600 MW PEG and 40 wt % AlSi. Other calcined AlSi notations are analogous.

Transmission electron microscopy (TEM) was performed using a JEOL 2010 FasTEM operated at 197 keV (3 keV offset from 200 keV using the Gatan Imaging Filter). The TEM was equipped with a Schottky field emission gun with a 0.9 eV energy spread and a 1.9 Å objective pole-piece. A Gatan energy filter with a 20 eV slit-width was used to select zero-loss electrons for the bright-field imaging of all samples. Images were captured using a Gatan 1024 × 1024 pixel CCD camera. Energy-dispersive X-ray spectroscopy (EDS) was done using an EDAX Phoenix X-ray spectrometer with a resolution of 134 eV. Samples were prepared by grinding the calcined samples using a mortar and pestle followed by suspension in acetone. A drop of the sample suspension was placed on a 3 mmΦ, 300-mesh copper grid coated with a lacey-carbon film (EMS Cat. #LC200-Cu). The acetone was then evaporated off at room temperature.

Thermal analysis was performed in air at 10°/min with a DuPont Instruments (Wilmington, DE) 951 Thermogravimetric Analyzer. Prior to analysis, the calcined samples were dried at 50 °C in a vacuum oven overnight.

Nitrogen sorption experiments were carried out at liquid nitrogen temperature using a Micromeritics ASAP 2010 instrument. Samples were degassed at 200 °C in vacuo for 12 h prior to investigation.

Solid-state (^{13}C, ^{29}Si, ^{27}Al) NMR measurements were performed as single pulse experiments on a Bruker DSX 400 MHz NMR spectrometer, using a 4 mm magic angle sample spinning (MAS) probe at a rate of 10 kHz. Rotation frequencies were stabilized with an active feedback spin-rate controller. The chemical shifts were referenced to glycine for ^{13}C, kaolin for ^{29}Si, and $AlCl_3$ for ^{27}Al. A 10 kHz MAS signal of ^{13}C was also acquired under non-CP, ^{1}H decoupled conditions in order to evaluate the sole contribution from carbon and test for the presence of free carbon and carbides. The decoupling conditions were optimized using glycine.

Impedance spectroscopy was used to measure the conductivity of OICM films. To maximize electrode−electrolyte contact, gold electrodes with a fixed area were sputtered directly onto the films using a Polaron E5100 sputter coater. Bulk resistances were extracted based on a parallel RC circuit model, using data measured with a HP 4192A impedance analyzer. Impedance data were obtained by sweeping the frequencies from 5 to 13 MHz, and subsequently converted to admittance form in order to fit the data and extrapolate bulk resistance.

Transference numbers were determined from slight modifications of the popular steady-state method, which entails polarizing a symmetric polymer electrolyte cell galvanostatically and assumes complete dissociation of the salt.[49] Since the observed

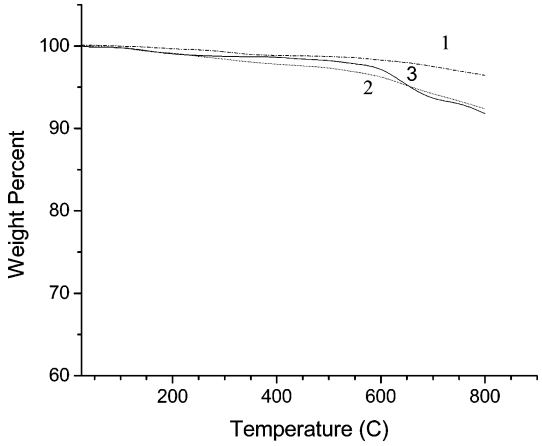

Figure 1. TGA curves of AlSi(6-70) (1), AlSi(6-55) (2), and AlSi-(6-40) (2).

voltage decay curve did not reflect a single relaxation process, the relaxation profile was split into two distinct regions with each one corresponding to either lithium ion or triflate ion relaxation. This enabled diffusion coefficients of each species to be estimated; subsequently, the lithium transference number was calculated by taking the fraction of the lithium diffusing through the electrolyte. "PEO + LiI" was used as a reference electrolyte with the lithium transference number (0.4) in reasonable agreement with published results (0.3).[50] Our results also agree with those based on the analogous system made by colleagues in another laboratory.[42]

Results and Discussion

TGA and NMR. Normally for mesoporous oxides templated over block polymers, prolonged calcination at 500 °C (as used in this work) results in practically complete decomposition of the organic template, which is usually confirmed by TGA.[46] To check completeness of the PEO removal in our samples, we examined AlSi(6-70), AlSi(6-55), and AlSi(6-40) by TGA. As shown in Figure 1, heating of Al(6-70) in air up to 800 °C results in an insignificant weight loss (about 3.5%), which usually confirms nearly entire removal of the organic phase.[46] Surprisingly, the TGA curves of AlSi(6-55) and AlSi(6-40) show weight losses up to 8% under the same conditions. One might suggest that the removal of the organic phase during calcination in these samples was impeded by the formation of closed pores.

Figures 2 and 3 present ^{29}Si and ^{27}Al NMR spectra, respectively, of the noncalcined PEG6-55 (Figures 2a and 3a) and calcined samples: AlSi(6-40) (Figures 2b and 3b), AlSi-(6-55) (Figures 2c and 3c), and AlSi(6-70) (Figures 2d and 3d). The aluminum spectrum of PEO6-55 shows two distinct sites at 0 and 51 ppm, indicating octahedral (six-coordinate) and tetrahedral (four-coordinate) coordination, respectively.[51] The aluminum spectrum of AlSi(6-55) (AlSi after calcination, Figure 3c) shows a significant decrease of the signal at 0 ppm (octahedral aluminum) and considerable increase and broadening of the signal assigned to tetrahedral Al. A noticeable increase of the intensity between these signals could be assigned to either a nonframework tetrahedral Al species in a highly distorted environment or a pentacoordinate species as reported in refs 52 and 53. At the same time, while the ^{27}Al NMR spectra of the noncalcined samples show no composition dependence (the spectra are identical for PEG6-40, PEG6-55 (shown), and PEG6-70), the spectra of their calcined products differ, depending on the composition. They show the same trend, described above for AlSi(6-55), i.e., changes of intensity and shape of the signals after calcination, but for AlSi(6-40), this change is rather negligible (Figure 3b), while for AlSi(6-70), it is more pronounced (Figure 3d) than for AlSi(6-55). The extra feature in Figure 3d at 12 ppm can be also ascribed to either a nonframework tetrahedral Al species or to pentacoordinate species as discussed above for AlSi(6-55).

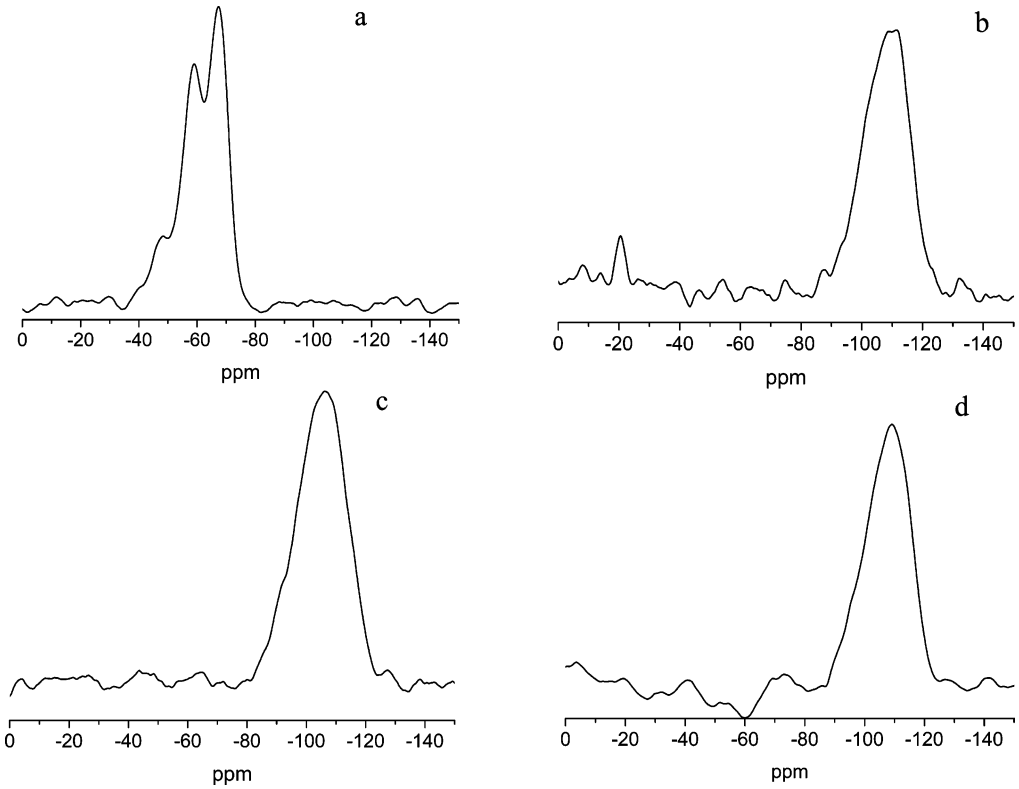

Figure 2. ^{29}Si MAS NMR of PEG6-55 (a), and AlSi(6-40) (b), AlSi(6-55) (c), and AlSi(6-70) (d).

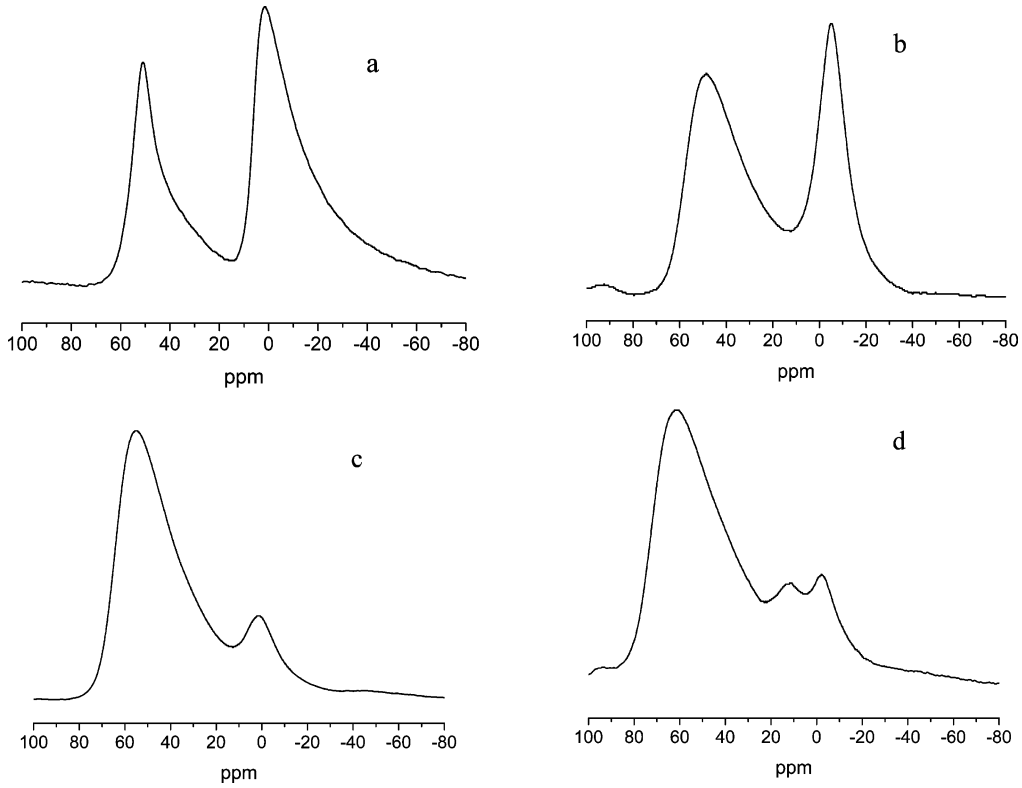

Figure 3. ^{27}Al MAS NMR spectra of PEG6-55 (a), AlSi(6-40) (b), AlSi(6-55) (c), and AlSi(6-70) (d).

The ^{29}Si NMR of AlSi(6-55) (Figure 2c) shows an upfield shift of all the signals (compared to PEO6-55, Figure 2a) due to removal of organic substituents at Si and transformation of T environments (organically modified silica) into Q environments (silica). The silicon spectrum of AlSi(6-55) is represented by a very broad signal, which should originate from the overlapping Q^3 and Q^4 signals at −100 and −110 ppm, respectively.[54] A signal intensity around −90 ppm should be attributed to Q^2 species.[55] This change is consistent with transformations observed in aluminosilica zeolites after calcination.[56−58] Comparison of the silicon spectra of PEO6-55 and AlSi(6-55) allows us to conclude that roughly T^1 {C−SiO-$(OH)_2$} converts to Q^2 {$SiO_2(OH)_2$}, T^2 {C−SiO_2(OH)} to Q^3 {SiO_3(OH)}, and T^3 {C−SiO_3} to Q^4 {SiO_4}. Since the preservation of the precursor material structure after calcination of OICM containing block copolymers and analogous aluminosilica was shown in refs 47 and 48, we assume that change of local environments of Al and Si does not affect the microstructure of the AlSi component on a nanometer scale. The ^{29}Si NMR spectrum of AlSi(6-70) (Figure 2d) is similar to that of AlSi(6-55), while the ^{29}Si NMR spectrum of AlSi(6-40) contains an additional small signal at 21 ppm which can be assigned to silicon carbide species.[59−61] The carbon (^{13}C) NMR spectrum of AlSi(6-40) (Figure 4a), recorded under 1H decoupled conditions (see experimental), shows a very broad signal with a maximum at about 100 ppm, two distinct narrow signals at 15.5 and 56.4 ppm, and a third signal at about 0 ppm. The signal at 15.5 ppm can be assigned to silicon carbide,[59,60] while the signal at 56.4 ppm may be associated with silicon oxycarbide species.[62] We have no assignment for the small resonance at 0 ppm at present. The broad signal at 100 ppm can be assigned to sp^3-like carbon obtained under high-pressure conditions (formed in the closed pores during calcination at 500 °C).[62,63] High intensity of the signal in the range 120−150 ppm can be assigned to sp^2-carbon.[62,63] Further heating (above 500 °C) of this sample during TGA examination results in opening the pores and the additional weight loss due to carbon oxidation observed by TGA. In the ^{13}C NMR spectrum of Al(6-55), the signals assigned to silicon carbide and oxycarbide species are absent (in agreement with ^{29}Si NMR data), while a broad signal associated with free carbon is evident, explaining the similar TGA weight losses for the Al(6-40) and Al(6-55) samples. Since free carbon is nearly "transparent" for TEM, the presence of these species in aluminosilica does not impede the accurate TEM examination.

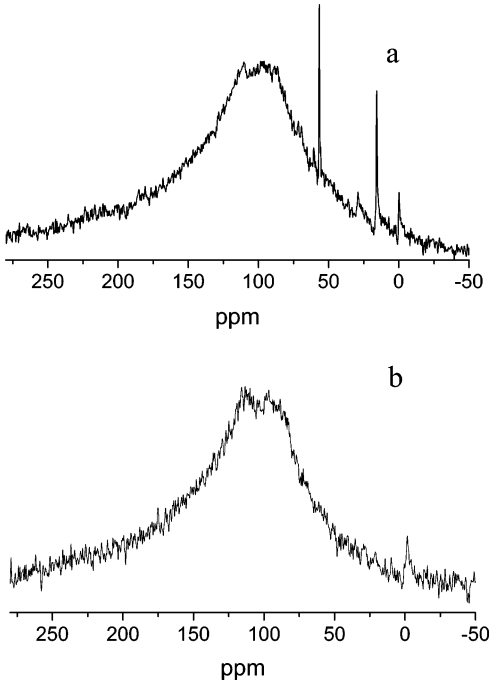

Figure 4. ^{13}C NMR spectra of Al(6-40) (a) and Al(6-55) (b). 10 kHz MAS signal was acquired under non-CP, ^{1}H decoupled conditions.

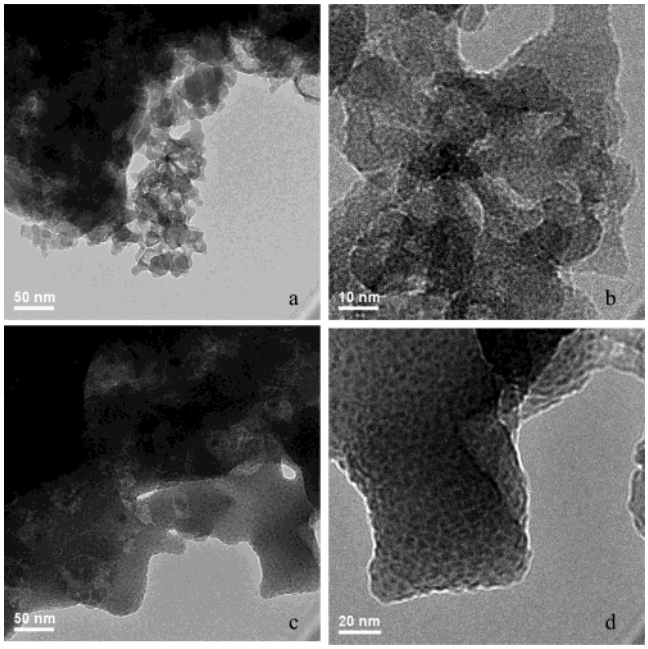

Figure 5. TEM images of calcined AlSi(6-40): (a) and (b) show particles, while (c) and (d) show platelets.

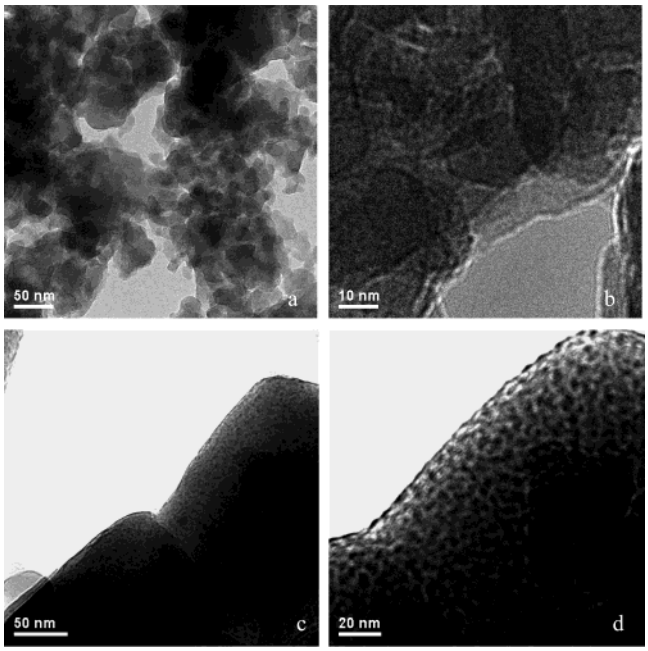

Figure 6. TEM images of calcined AlSi(6-55): (a) and (b) show particles, and (c) and (d) show platelets.

TEM. Figures 5−8 show the TEM images of calcined AlSi derived from OICM of different composition and structure. The major feature of all calcined AlSi based on 600 MW PEO and prepared by casting on a Teflon dish is the presence of two types of morphologies: nanoparticles with sizes of about 20−60 nm and much larger platelike particles (Figure 5c,d). Increasing the amount of AlSi in OICM increases the fraction of platelike particles relative to nanoparticles. In the sample containing 70 wt % AlSi in OICM, nanoparticles are nearly absent. Another interesting feature is that the porosity of these two kinds of AlSi particles is different. The nanoparticles are practically nonporous, while platelets are considerably mesoporous. The TEM images show a disordered arrangement of mesopores. The pore disorder is confirmed by the diffuse scattering observed in the selected area electron diffraction

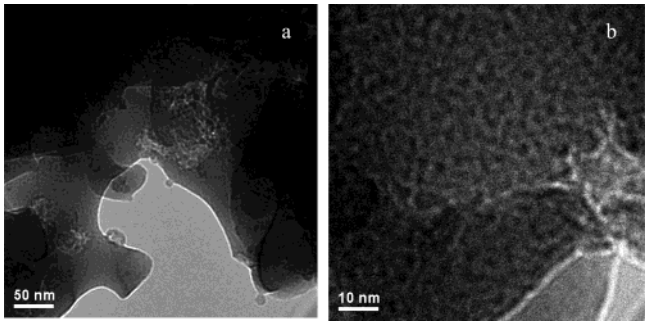

Figure 7. TEM images of calcined AlSi(6-70). Here (a) and (b) show platelets. Particles are not shown as they represent a small fraction of material.

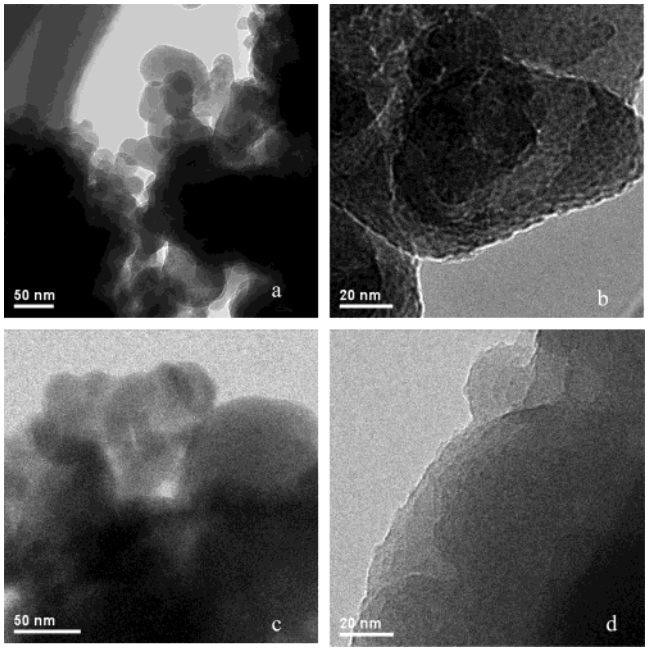

Figure 8. TEM images of calcined AlSi(6-55) derived from the film prepared by spin coating (a and b) and AlSi(1000-55) (c and d) obtained by casting.

(SAED) patterns, with no observable Bragg reflections or polycrystalline rings. Unlike the amphiphilic block copolymer templates creating mesopore ordering,[47] PEO aggregation occurs randomly. It is noteworthy that pores in the bright-field images presented here appear as dark spots due to the phase contrast transfer function at the level of defocus used in imaging (other studies[47,48] have reported these pores to appear as light regions in bright-field images).

On average, the diameter of mesopores measures 2.9 nm in AlSi(6-40), 3.2 nm in AlSi(6-55), and 2.2 nm in AlSi(6-70). One can see that these values are inconsistent with the estimation of the mobile domain size from ^{1}H spin diffusion measurements.[43] We assume that the mobile PEO domains are formed between nanoparticles and/or platelets and that they are responsible for Li ion mobility in OICM, while 2−3 nm "PEO + LiTf islands", formed inside the AlSi platelets, do not contribute in the PEO mobility and do not influence the conductivity.

When an OICM film is prepared by spin coating (Figure 8a,b), both nanoparticles and platelets have similar porosity with a mean pore size of 1.3 nm. Apparently, spin coating leads to a more homogeneous AlSi phase in the OICM. When 100 000 MW PEO is employed instead of low-molecular-weight PEG (600 MW), AlSi is represented by mainly platelets with no porosity. Here AlSi structure is similar for cast and spin-coated

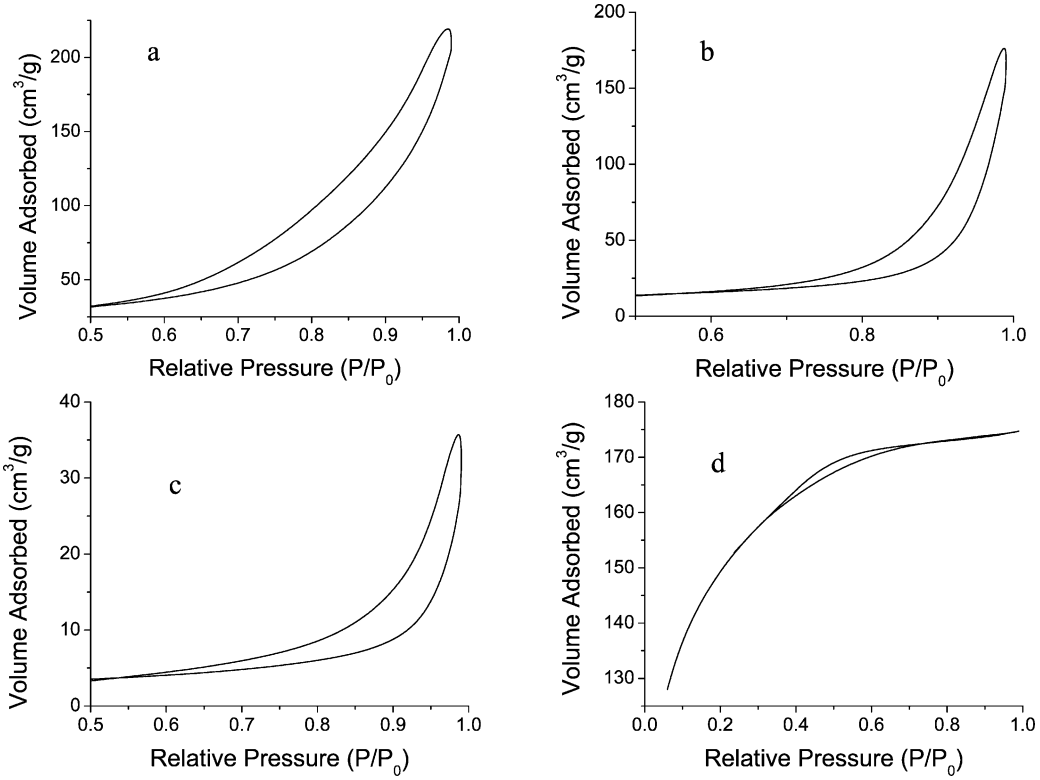

Figure 9. N_2 adsorption−desorption isotherms of calcined AlSi(6-40) (a), AlSi(6-55) (b), AlSi(6-70) (c), and AlSi(6-55) derived from OICM with no LiTf (d).

films. The difference between samples based on 600 MW and 100 000 MW polymers can be explained by the macromolecule sizes: the PEG and PEO coil sizes calculated using square root law[64] are ∼1 and 17 nm, respectively. Thus, small PEG molecules with only ∼14 repeating units easily penetrate into the precondensed AlSi even when they coordinate with LiTf, while high-molecular-weight PEO molecules (∼2270 repeating units) appear to be larger than the possible pores in the precondensed AlSi.

The EDS analysis indicates that the Al/Si ratio varies between 1:5 and 1:6 in the calcined AlSi based on 600 MW PEG, while in the noncalcined samples the A/Si ratio is 1:4. The calcined AlSi samples derived from 100 000 MW PEO have a lower Al/Si ratio, varying between 1:7 and 1:9. Partial dealumination during calcination is described in ref 65. The interesting phenomenon here is a different degree of dealumination in the samples based on low-molecular-weight PEG and high-molecular-weight PEO. We think that penetration of PEG molecules inside the AlSi (for OICM based on 600 MW PEG) prevents significant dealumination and better preserves the AlSi structure.

Nitrogen Adsorption. Nitrogen adsorption is a standard and commonly used technique for specific surface evaluation.[66] The shapes of N_2 adsorption−desorption isotherms and hysteresis loops also provide important qualitative information on the presence or absence of micropores and the type of mesoporosity.[66] The N_2 adsorption−desorption isotherms of AlSi obtained after calcination of cast PEG6-40, PEG6-55, PEG6-70, and spin-coated PEG6-55 are presented in Figure 9a−d. One can see that the shape of isotherms for all these samples is similar to the H3 type discussed in ref 66 and attributed to aggregates (loose assemblages) of platelike particles forming slitlike pores. The N_2 adsorption−desorption isotherms of nonporous AlSi-(1000-55) samples (the lack of internal pores was shown by TEM) based on both cast and spin-coated samples are similar to those shown in Figure 9.

TABLE 1: Nitrogen Adsorption Data for Calcined OICM

AlSi based on[a]	BET surface, $m^2\ g^{-1}$	pore volume, $cm^3\ g^{-1}$	external surface, $m^2\ g^{-1}$
PEG6-40	80.4	0.34	79.1
PEG6-55	36.1	0.27	43.8
PEG6-70	9.6	0.06	9.6
PEG6-70 without LiTf	521.1	0.27	300.9
PEG6-55, spin coating	38.2	0.29	44.2
PEO1000-55	26.2	0.18	25.5

[a] If not indicated otherwise, the OICM films were prepared by casting from reaction solution on a Teflon dish.

As seen from Table 1, the values of the BET (Brunauer-Emmet-Teller) surface area are considerably lower than values reported for mesoporous materials with pore sizes of about 3 nm.[67] This might be caused by only partial porosity of the calcined AlSi; as observed by TEM, AlSi nanoparticles are not porous. Another possible reason is the formation of fully or partially closed pores. Since the BET surface areas for these samples are practically equal to the external surface areas, i.e., the surface of nanoparticles and platelets (Table 1), we assume that BJH (Barrett, Joyner, and Halenda) pore size distributions describe only pores formed between AlSi particles and/or platelets, while pores located inside the AlSi must be closed. The shape similarity of the N_2 adsorption−desorption isotherms of the calcined AlSi's based on PEG6 (mesoporous) and PEO1000 (nonporous), confirms this conclusion. The blockage of the pores may occur due to the presence of LiTf. Insertion of Li in metal oxides during calcination at 500 °C is described elsewhere.[68] We believe that during calcination, removal of the organic component and insertion of Li species in the inorganic framework is accompanied by closing of the pore entrance. For PEO6-40 and PEO6-55 containing the larger relative LiTf contents, the blockage of the pores happens even earlier than when the organic component is fully removed. This may explain

TABLE 2: Conductivities and Li Transference Numbers for OICM Films

AlSi based on[a]	conductivity,[b] S cm^{-1}	Li transference number
PEG6-40	2.67×10^{-5}	0.7
PEG6-55	1.65×10^{-5}	0.6
PEG6-70	9.71×10^{-7}	0.5
PEG6-55, spin coating	1.48×10^{-5}	0.3
PEO1000-55	7.00×10^{-6}	0.7

[a] If not indicated otherwise, the OICM films were prepared by casting from reaction solution on Teflon dish. [b] Conductivity was acquired at room temperature.

the presence of ~8% volatile species in AlSi(6-40) and AlSi-(6-55) as observed by TGA (Figure 1). Apparently, in the PEO6-70 sample, the blockage occurs after complete removal of the organic component.

When LiTf is not added to OICM, the N_2 adsorption−desorption isotherms of calcined AlSi show completely different patterns, with large adsorption at low relative pressures and small hysteresis loops, which are evidence of high microporosity and low mesoporosity of this sample (Figure 9d). Thus, in the absence of LiTf, PEO does not aggregate, so mesopores are not likely to form. This is in a good agreement with the findings of ref 69, where silica templating over 100 000 MW PEO resulted mainly in microporous material. The unusually high external surface area of this sample (Table 1) is due to formation of microporous nanoparticles of 30−35 nm in diameter instead of large platelets shown in Figure 7. In contrast, AlSi obtained after calcination of Li-containing OICM shows no microporosity. This can be due to either absence of free PEO chains (interaction with LiTf causes aggregation) during templating or to blockage of the micropores along with the mesopores.

Conductivity. From the TEM data, one can see that when the AlSi content in OICM is higher (in the range 40−70 wt %), the fraction of nanoparticles is lower, while large platelike particles prevail. This leads to a decrease in the external surface area (as shown by the BET data), which indicates a decrease of the interfacial surface in the noncalcined OICM. To find a relationship between interfacial surface areas and electrochemical properties of the corresponding OICM, we measured conductivities and Li transference numbers of the SPE films discussed in this paper (Table 2). Comparison of the data presented in Tables 1 and 2 shows that there is a correlation between the external surface area of the calcined AlSi and conductivity. The highest conductivity is observed for PEG6-40 film and the highest surface area is found for the Al(6-40) sample. The lowest SPE conductivity and the lowest surface area of the calcined AlSi are found for PEG6-70. In general, an increased fraction of AlSi nanoparticles vs platelets provides both higher interfacial surface and higher conductivity.

Unlike conductivity, correlation between interfacial surface areas and Li transference numbers is less obvious. For the cast PEG6 samples, we see the same dependence: the higher the external surface area, the higher the transference numbers and conductivity. This suggests that the interfacial surface plays an important role in the enhancement of Li transport numbers in OICM along with conductivity. This is inconsistent with the findings of ref 70, which reported little effect of the filler particles on the "free" anion/ion-pair/higher aggregate equilibrium, i.e., Li transference numbers. This difference comes from the fact that in ref 70, the authors used preformed fillers in which the external surfaces were already "contaminated" with stabilizing reagents or impurities, whereas the AlSi particles, originated here, form within the "PEO + LiTf" phase, thus a "clean" interface is exposed to Li salt during formation.

At the same time, the Li transference number of the spin-coated PEG6-55 is much lower than that of the cast sample, though the surface area values are similar. It is worth mentioning that from TEM, the AlSi structure of the spin-coated film is quite different from that of the cast samples. The high Li transference number of the PEO1000-55 film is also inconsistent with the comparatively low external surface area. On that basis, one might suggest that Li transference numbers are determined both by the size of the interfacial surface area and by the types of the Si and Al sites present at the interface. Since calcination changes the local environment of Si and Al sites, they cannot be studied in the calcined OICM and will be a subject of a separate study.

Conclusions

By means of solid-state NMR, TEM, and nitrogen adsorption, we studied the structure of AlSi domains formed in situ by a sol−gel process within the "PEO (PEG) + Li triflate" component of OICM. ^{29}Si MAS NMR spectra show that transition of OICM into AlSi is accompanied with conversion of T^1 to Q^2, T^2 to Q^3, and T^3 to Q^4, confirming that the overall structure on the nanometer scale remains the same, although local Si and Al structure changes. TEM shows that AlSi structure strongly depends on the polymer molecular weight, amount of the AlSi component, and the method of SPE film preparation. In OICM films based on 600 MW PEG and obtained by casting on a Teflon dish, AlSi's contain two types of structures: nanoparticles of 20−60 nm in size and larger platelike particles. Increase of the AlSi fraction in OICM results in the decrease of nanoparticle fraction, so large platelets prevail. In so doing, nanoparticles are practically nonporous, while platelets are considerably mesoporous. Spin coating results in OICM films with more homogeneous AlSi domains containing smaller pores. At the same time, all these pores seem to be closed (the BET surface area for each AlSi sample is equal to the external surface area), thus "PEG + LiTf" domains, formed inside the AlSi network, do not contribute to Li ion conductivity or transference numbers. AlSi's based on 100 000 MW PEO consists of nonporous platelets independently of the way of the SPE film preparation. Conductivity measurements show that the increase of AlSi surface area is consistent with an increase of conductivity, while Li transference numbers change in a more complicated pattern.

Acknowledgment. The authors thank NASA for Grant NAG3-2588 for financial support of this project and Dr. Paul Schettler (Department of Chemistry, Juniata College, Huntingdon, PA 16654) for allowing use of the porosimeter.

References and Notes

(1) Sanchez, C.; de Soler-Illia, G. J.; Ribot, F.; Lalot, T.; Mayer, C. R.; Cabuil, V. *Chem. Mater.* **2001**, *13*, 3061.
(2) Shea, K. J.; Loy, D. A. *Chem. Mater.* **2001**, *13*, 3306.
(3) Cerveau, G.; Corriu, R. J. P.; Framery, E. *Chem. Mater.* **2001**, *13*, 3373.
(4) Schottner, G. *Chem. Mater.* **2001**, *13*, 3422.
(5) Pyun, J.; Matyjaszewski, K. *Chem. Mater.* **2001**, *13*, 3436.
(6) Schubert, U. *Chem. Mater.* **2001**, *13*, 3487.
(7) Ahmad, Z.; Mark, J. E. *Chem. Mater.* **2001**, *13*, 3320.
(8) Bronstein, L. M.; Joo, C.; Karlinsey, R.; Ryder, A.; Zwanziger, J. W. *Chem. Mater.* **2001**, *13*, 3678.
(9) Manias, E.; Touny, A.; Wu, L.; Strawhecker, K.; Lu, B.; Chung, T. C. *Chem. Mater.* **2001**, *13*, 3516.
(10) Antonietti, M.; Breulmann, M.; Göltner, C. G.; Cölfen, H.; Wong, K. K. W.; Walsh, D.; Mann, S. *Chem.-A Eur. J.* **1998**, *4*, 2493.
(11) Watson, K. J.; Zhu, J.; Nguyen, S. B. T.; Mirkin, C. A. *J. Am. Chem. Soc.* **1999**, *121*, 462.
(12) Förster, S.; Antonietti, M. *Adv. Mater.* **1998**, *10*, 195.

(13) Silva, A. S.; Mitchell, C. A.; Fu Tse, M.; Wang, H.-C.; Krishnamoorti, R. *J. Chem. Phys.* **2001**, *115*, 7166.
(14) Antonietti, M.; Wenz, E.; Bronstein, L.; Seregina, M. *Adv. Mater.* **1995**, *7*, 1000.
(15) Spatz, J. P.; Roescher, A.; Möller, M. *Adv. Mater.* **1996**, *8*, 337.
(16) Yan, X.; Liu, G.; Liu, F.; Tang, B. Z.; Peng, H.; Pakhomov, A. B.; Wong, C. Y. A. C. *Angew. Chem., Int. Ed.* **2001**, *40*, 3593.
(17) Steunou, N.; Foerster, S.; Florian, P.; Sanchez, C.; Antonietti, M. *J. Mater. Chem.* **2002**, *12*, 3426.
(18) Sohn, B. H.; Cohen, R. E.; Papaefthymiou, G. C. *J. Magn. Magn. Mater.* **1998**, *182*, 216.
(19) Croce, F.; Appetecchi, G. B.; Persi, L.; Scrosati, B. *Nature* **1998**, *394* (6692), 456.
(20) Cummins, C. C.; Schrock, R. R.; Cohen, R. E. *Chem. Mater.* **1992**, *4*, 27.
(21) Fogg, D. E.; Radzilowski, L. H.; Dabbousi, B. O.; Schrock, R. R.; Thomas, E. L.; Bawendi, M. G. *Macromolecules* **1997**, *30*, 8433.
(22) Moffitt, M.; McMahon, L.; Pessel, V.; Eisenberg, A. *Chem. Mater.* **1995**, *7*, 1185.
(23) Zoppi, R. A.; Soares, C. G. A. *Adv. Polym. Technol.* **2002**, *21*, 2.
(24) Matejka, L. *MRS Symp. Proc.* **2002**, *726*, 57.
(25) Kickelbick, G. *Prog. Polym. Sci.* **2002**, *28*, 83.
(26) Yang, S.; Horibe, Y.; Chen, C.-H.; Mirau, P.; Tairy, T. *Polym. Prepr.* **2002**, *43* (2), 386.
(27) Hutchison, J. C.; Bissessur, R.; Shriver, D. F. *MRS Symp. Proc.* **1997**, *457*, 489.
(28) Scrosati, B. *Chem. Record* **2001**, *1*, 173.
(29) Dahmouche, K.; Atik, M.; Mello, N. C.; Bonagamba, T. J.; Panepucci, H.; Judeinstein, P.; Aegerter, M. A. *Ceram. Trans.* **1998**, *81*, 311.
(30) Abraham, K. M.; Koch, V. R.; Blakley, T. J. *J. Electrochem. Soc.* **2000**, *147*, 1251.
(31) Ulrich, R.; Zwanziger, J. W.; De Paul, S. M.; Richert, R.; Wiesner, U.; Spiess, H. W. *Polym. Mater. Sci. Eng.* **1999**, *80*, 610.
(32) de Souza, P. H.; Bianchi, R. F.; Dahmouche, K.; Judeinstein, P.; Faria, R. M.; Bonagamba, T. J. *Chem. Mater.* **2001**, *13*, 3685.
(33) Kohjiya, S.; Kitade, T.; Ikeda, Y.; Hayashi, A.; Matsuda, A.; Tatsumisago, M.; Minami, T. *Solid State Ionics* **2002**, *154*−*155*, 1.
(34) Krawiec, W.; Scanlon, L. G. J.; Fellner, J. P.; Vaia, R. A.; Vasudevan, S.; Giannelis, E. P. *J. Power Sources* **1995**, *54*, 310.
(35) Giannelis, E. P. *Adv. Mater.* **1996**, *8*, 29.
(36) Chu, P. P.; Reddy, M. J.; Kao, H. M. *Solid State Ionics* **2003**, *156*, 141.
(37) Brik, M. E.; Titman, J. J.; Bayle, J. P.; Judeinstein, P. *J. Polymer. Sci. Polym. Phys.* **1996**, *34*, 2533.
(38) De Paul, S. M.; Zwanziger, J. W.; Ulrich, R.; Wiesner, U.; Spiess, H. W. *J. Am. Chem. Soc.* **1999**, *121*, 5727.
(39) Wieczorek, W.; Such, K.; Chung, S. H.; Stevens, J. R. *J. Phys. Chem.* **1994**, *98*, 9047.
(40) Golodnitsky, D.; Ardel, G.; Peled, E. *Solid State Ionics* **2002**, *147*, 141.
(41) Croce, F.; Curini, R.; Martinelli, A.; Persi, L.; Ronci, F.; Scrosati, B.; Caminiti, R. *J. Phys. Chem. B* **1999**, *103*, 10632.
(42) Ulrich, R.; Zwanziger, J. W.; De Paul, S. M.; Reiche, A.; Leuninger, H.; Spies, H. W.; Wiesner, U. *Adv. Mater.* **2002**, *14*, 1134.
(43) Joo, C. G.; Bronstein, L. M.; Karlinsey, R. L.; Zwanziger, J. W. *Solid State Nucl. Magn. Reson.* **2002**, *22*, 235.
(44) Schmid, G., Ed. *Clusters and Colloids: From Theory to Applications*; VCH: Weinheim, Germany, 1994.
(45) Templin, M.; Wiesner, U.; Spies, H. W. *Adv. Mater.* **1997**, *9*, 814.
(46) Göltner, C. G.; Henke, S.; Weissenberger, M. C.; Antonietti, M. *Angew. Chem., Int. Ed.* **1998**, *37*, 613.
(47) Finnefrock, A. C.; Ulrich, R.; Du Chesne, A.; Honeker, C. C.; Schumacher, K.; Unger, K. K.; Gruner, S. M.; Wiesner, U. *Angew. Chem., Int. Ed.* **2001**, *40*, 1208.
(48) Simon, P. F. W.; Ulrich, R.; Spies, H. W.; Wiesner, U. *Chem. Mater.* **2002**, *13*, 3464.
(49) Bruce, P. G.; Vincent, C. A. *Faraday Discuss. Chem. Soc.* **1989**, *88*, 43.
(50) Bouridah, A.; Dalard, F.; Deroo, D.; Armand, M. B. *Solid State Ionics* **1986**, *18&19*, 287.
(51) Chaudhari, K.; Das, T. K.; Chandwadkar, A. J.; Sivasanker, S. *J. Catal.* **1999**, *186*.
(52) Ray, G. J.; Meyers, B. L.; Marshall, C. L. *Zeolites* **1987**, *7*, 307.
(53) Selvaraj, U.; Komarneni, S.; Roy, R. *J. Am. Ceram. Soc.* **1990**, *73*, 3663.
(54) Ogura, M.; Kawazu, Y.; Takahashi, H.; Okubo, T. *Chem. Mater.*, in press.
(55) Janes, N.; Oldfield, E. *J. Am. Chem. Soc.* **1985**, *107*, 6769.
(56) Lawton, S. L.; Fung, A. S.; Kennedy, G. J.; Alemany, L. B.; Chang, C. D.; Hatzikos, G. H.; Lissy, D. N.; Rubin, M. K.; Timken, H.-K. C. *J. Phys. Chem.* **1996**, *100*, 3788.
(57) Romero, A. A.; Alba, M. D.; Klinowski, J. *J. Phys. Chem.* **1998**, *102*, 123.
(58) Agundez, J.; Diaz, I.; Marquez-Alvarez, C.; Perez-Pariente, J.; Sastre, E. *Chem. Commun.* **2003**, 150.
(59) Wagner, G. W.; Na, B. K.; Vannice, M. A. *J. Phys. Chem.* **1989**, *93*, 5061.
(60) Guth, J. R.; Petuskey, W. T. *J. Phys. Chem.* **1987**, *91*, 5361.
(61) Freitas, J. C. C.; Emmerich, F. G.; Bonagamba, T. J. *Chem. Mater.* **2000**, *12*, 711.
(62) Suyal, N.; Hoebbel, D.; Mennig, M.; Schmidt, H. *J. Mater. Chem.* **1999**, *9*, 3061.
(63) Trassl, S.; Kleebe, H.-J.; Stormer, H.; Motz, G.; Rossler, E.; Ziegler, G. *J. Am. Ceram. Soc.* **2002**, *85*, 1268.
(64) Grosberg, A. Y.; Khokhlov, A. R. *Statistical Physics of Macromolecules*; AIP: New York, 1994.
(65) Villaescusa, L. A.; Barrett, P. A.; Kalwei, M.; Koller, H.; Camblor, M. A. *Chem. Mater.* **2001**, *13*, 2332.
(66) Kruk, M.; Jaroniec, M. *Chem. Mater.* **2001**, *13*, 3169.
(67) Göltner, C. G.; Smarsly, B.; Berton, B.; Antonietti, M. *Chem. Mater.* **2001**, *13*, 1617.
(68) Doeff, M. M.; Richardson, T. J.; Kepley, L. *J. Electrochem. Soc.* **1996**, *143*, 2507.
(69) Goeltner, C. G.; Smarsly, B.; Berton, B.; Antonietti, M. *Chem. Mater.* **2001**, *13*, 1617.
(70) Johansson, P.; Ratner, M.; Shriver, D. F. *J. Phys. Chem. B* **2001**, *105*, 9016.